Supplementary Information

Electrodeposited-Film Electrodes Derived from A Precursor Dinitrosyl Iron Complex for Electrocatalytic Water Splitting

Wei-Liang Li,[†] Tzung-Wen Chiou,[†*] Chien-Hong Chen,[‡] Yi-Ju Yu,[†] Li-Kang Chu[†] and Wen-Feng Liaw[†*]

[†]Department of Chemistry, National Tsing Hua University, Hsinchu 30013, Taiwan
[‡]Department of Medical Applied Chemistry, Chung Shan Medical University and Department of Medical Education, Chung Shan Medical University Hospital, Taichung 40201, Taiwan

* e-mail: d9623817@oz.nthu.edu.tw (TWC) & wfliaw@mx.nthu.edu.tw (WFL)

Experimental Section

Manipulations, reactions, and transfers were conducted under N_2 according to Schlenk techniques or in a glovebox (N_2 gas). Solvents were distilled under N_2 from appropriate drying agents (diethyl ether from CaH_2; acetonitrile from CaH_2/P_2O_5; methylene chloride from CaH_2; hexane and THF from sodium benzophenone) and stored in dried, N_2-filled flasks over 4-Å molecular sieves. N_2 was purged through these solvents before use. The solvent was transferred to the reaction vessel via a stainless cannula under positive pressure of N_2. The reagents and materials iron pentacarbonyl, nitrosonium tetrafluoroborate [NO][BF$_4$], nitrosonium hexafluoroantimonate [NO][SbF$_6$], tris[2-(dimethylamino)ethyl]amine (Me$_6$tren), platinum on carbon (40 wt. % Pt/C, Pt on an activated carbon support), 99.9% IrO$_2$ powder, Nafion® perfluorinated resin solution (5 wt. % in lower aliphatic alcohols and water, contains 15-20% water) (Sigma-Aldrich), FeCl$_2$, FeCl$_3$, Fe$_2$(SO$_4$)$_3$, Fe(NO$_3$)$_3$ (Alfa Aesar), bis(triphenylphosphoranylidene)ammonium chloride ([PPN][Cl]; Fluka), platinum disk electrode (surface area = 0.0707 cm^2) (ALS), glassy carbon disk electrode (surface area = 0.0707 cm^2, CH instruments), graphite plate (R8340, 50×4×1 mm, 12 μΩm resistivity, Great Carbon Co., Ltd., Taiwan) were used as received. Compounds [PPN][Fe(CO)$_3$(NO)], [Fe(CO)$_2$(NO)$_2$], and [(PMDTA)Fe(NO)$_2$][BF$_4$] (PMDTA = pentamethyldiethylenetetraamine) were synthesized based on the reported procedures.[1-2] IR and ATR-IR spectra of the $\nu_{(NO)}$ stretching frequencies were recorded on a PerkinElmer model spectrum one B spectrometer with sealed solution cells (0.1 mm, CaF$_2$ windows) and a VERTEX 80 BioATRII. ^{1}H NMR spectra were obtained on a Varian Unity-500 spectrometer. UV-vis spectra were recorded on a Jasco V-570 spectrometer. Analyses of C, H, and N were obtained with a CHN analyzer (Heraeus).

Preparation of [(Me$_6$tren)Fe(NO)$_2$] (1) (Me$_6$tren = tris[2-

(dimethylamino)ethyl]amine). Ligand Me_6tren (0.30 mL, 1.1 mmol) was added into the THF solution (10 mL) of $[Fe(CO)_2(NO)_2]$, freshly prepared from reaction of $[PPN][Fe(CO)_3(NO)]$ (0.712 g, 1.0 mmol) and $[NO][BF_4]$ (0.120 g, 1.1 mmol), and the reaction solution was stirred for 4 h under N_2 at ambient temperature. The reaction was monitored with FTIR. The appearance of IR $\nu_{(NO)}$ stretching frequencies at 1697, 1643 cm^{-1} (THF) was assigned to the formation of $[(Me_6tren)Fe(NO)_2]$ (**1**). Complex **1** was isolated as dark brown semi-oil. IR: $\nu_{(NO)}$ 1697, 1643 cm^{-1} (THF). ^1H NMR (C_4D_8O): δ 2.47 (br (CH_2, CH_3)).

Preparation of $[(Me_6tren)Fe(NO)_2][SbF_6]$ (2). To a 30-mL Schlenk flask loaded with $[NO][SbF_6]$ (or $[NO][BF_4]$) (0.292 g (or 0.120 g), 1.1 mmol) was added the MeCN solution (10 mL) of complex **1** (0.346 g, 1.0 mmol). After stirring for 10 min, the shift of IR $\nu_{(NO)}$ stretching frequencies from 1689, 1633 cm^{-1} to 1765, 1679 cm^{-1} indicates the formation of $[(Me_6tren)Fe(NO)_2][SbF_6]$ (**2**). The MeCN solution of **2** was then filtered through Celite to remove the insoluble solid. The THF-diethyl ether was added to precipitate the brown solid **2**. Recrystallization from the MeCN solution of complex **2** layered with diethyl ether at room temperature led to the dark brown crystals suitable for X-ray crystallography. IR: $\nu_{(NO)}$ 1765, 1679 cm^{-1} (MeCN). Absorption spectrum (MeCN) [λ_{max}, nm (ε, $M^{-1}cm^{-1}$)]: 386 (454), 513 (147), 670 (72), 833 (64). Anal. Calcd. for $C_{12}H_{30}FeN_6O_2F_6Sb$: C, 24.76; H, 5.20; N, 14.44. Found: C, 23.69; H, 5.15; N, 14.13.

EPR Spectroscopy. EPR measurements were performed at X-band using a Bruker EMX spectrometer equipped with a Bruker TE102 cavity. The microwave frequency was measured with a Hewlett-Packard 5246L electronic counter. X-band EPR spectrum of **2** in MeCN was obtained with a microwave power of 1.5 mW, modulation amplitude of 1.60 G at 100 KHz, and microwave frequency at 9.469 GHz. The spectral simulation was performed using Bruker WinEPR.

Magnetic Measurements. The magnetization data was recorded on a SQUID magnetometer (MPMS5 Quantum Design company) with an external 1.0 T magnetic field for **2** in the temperature range 2-300 K. The magnetic susceptibility of the experimental data was corrected for diamagnetism by the tabulated Pascal's constants.

Crystallography. Each crystal was mounted on a glass fiber and quickly coated with an epoxy resin. Unit-cell parameters were obtained by least-squares refinement. Diffraction measurement for complex **2** was carried out on a Bruker Kappa Apex DUO diffractometer (Brucker X8 APEX II CCD diffractometer) with graphite-monochromated Mo K_α radiation (λ = 0.7107 Å). Least-squares refinement of the positional and anisotropic thermal parameters of all non-H atoms and fixed H atoms was based on F^2. A *SADABS* absorption correction was made. The *SHELXTL* structural refinement program was employed. CCDC number: CCDC 1559817 for **2**.

Electrode Preparation. 40 wt.% Pt-C (3.6 mg) or IrO_2 (2.1 mg) were dispersed in a 2 mL mixture solution containing 0.8 mL water, 120 μL 5% Nafion solution, and 1.08 mL ethanol, followed by sonication for 30 min to obtain a homogeneous catalyst ink. The catalyst ink (50 μL for each loading) was loaded on the surfaces of the glassy carbon electrode (surface area: 0.0707 cm^2) or graphite plate (surface area: 0.16 cm^2) to achieve the suitable weight.[3]

Electrochemical Studies. All electrochemical measurements were performed in a three-electrode cell with a CHI model 621b potentiostat (CH Instrument) instrumentation. Cyclic voltammograms in MeOH were obtained from 3.0 mM analyte concentration in O_2-free MeOH using 0.1 M [n-Bu$_4$N][PF$_6$] as the supporting electrolyte. The potential was measured at 298 K vs Ag/AgNO$_3$ reference electrode (0.01 M AgNO$_3$, ALS) by using a glassy carbon working electrode (surface area = 0.0707 cm^2) and a platinum wire auxiliary electrode (ALS) at a scan rate of 50 mV/s. The working electrode was polished with Al$_2$O$_3$ powders with size down to 0.05 μm.

The potentials are reported against the ferrocenium/ferrocene (Fc$^+$/Fc) couple. In all experiments, the iR compensation was performed by CHI model 621b software. Aqueous cyclic voltammogram (CV) and linear sweep voltammetry (LSV) were obtained from 3.0 mM analyte concentration in 1.0 M NaOH as the supporting electrolyte with the saturated calomel electrode (SCE, ALS) as reference electrode at a scan rate of 2 mV/s. Controlled potential electrolysis (CPE) experiments of complex **2** solution (3.0 mM) were conducted in 25-mL 1.0 M NaOH aqueous solution stirred constantly. The auxiliary electrode in CPE cell was separated from the solution of the working electrode by a medium-porosity sintered-glass frit. To avoid the corrosion of the expensive glassy carbon electrode, graphite plate (surface area = 0.16 cm^2) was used as the working electrode in the CPE experiments of water oxidation and two-electrode setting. All potentials reported in this paper were converted from vs SCE to vs reversible hydrogen electrode (RHE).

$$RHE = SCE + 0.244 + 0.059 \times 14, \text{ for 1.0 M NaOH}_{(aq)}$$

Electrochemical Capacitance Measurements. The electrochemically active surface area (ECSA) was evaluated in terms of double-layer capacitance. CV scans were conducted in static solution by sweeping the potential from the more positive to negative potential and back at 6 different scan rates: 2, 4, 8, 12, 16 and 20 mV/s. This range is typically a 0.1 V potential window centered on the OCP (open-circuit potential) of the system. The capacitance was determined from the tenth cyclic voltammetry curve of each scan rate. The electrochemical double-layer capacitance, C_{DL}, as given by $i_c = v C_{DL}$ (i_c: current density from CV, v: scan rate).[4] The specific capacitance for a flat surface is generally found to be in the range of 20-60 mF/cm^2. We used a value of 40 mF/cm^2 in the following calculations of the electrochemical

active surface area.

Mass Activity. The values of mass activity were calculated using the equation, mass activity (A/g) = LSV current (A)/electrocatalyst deposited or loading amount (g).

Determination of Faradaic Efficiency, TON and TOF of Electrolysis Using DNIC 2-Deposited Electrode. Quantification of the produced H_2/O_2 gas was performed by gas chromatography (SRI 8610C) equipped with a molecular sieves (MS-13x) column and helium ionization detector (HID). Helium was used as the carrier gas. Calibration curves were built by the injection of the known amounts of pure H_2/O_2. The amounts of H_2/O_2 dissolved in the solution were corrected by the Henry's law ($K_H = 7.8 \times 10^{-4}$ mol/atm·L for H_2 and 1.3×10^{-3} mol/atm·L for O_2).

H_2: *Faradaic efficiency* (%) = [Charge (CPE)/2/96485]×100%/[V(H_2 gas of GC detection)/24.5]

O_2: *Faradaic efficiency* (%) = [Charge (CPE)/4/96485]×100%/[V(O_2 gas of GC detection)/24.5]

TON (H_2) = [Q/2/96485]×[Faradaic efficiency (%)]/[weight of catalyst] (mol/g)

TON (O_2) = [Q/4/96485]×[Faradaic efficiency (%)]/[weight of catalyst] (mol/g)

Q = accumulated charge of CPE with catalyst − accumulated charge of CPE without catalyst

TOF = [TON]/[time of CPE] (mol/g-h)
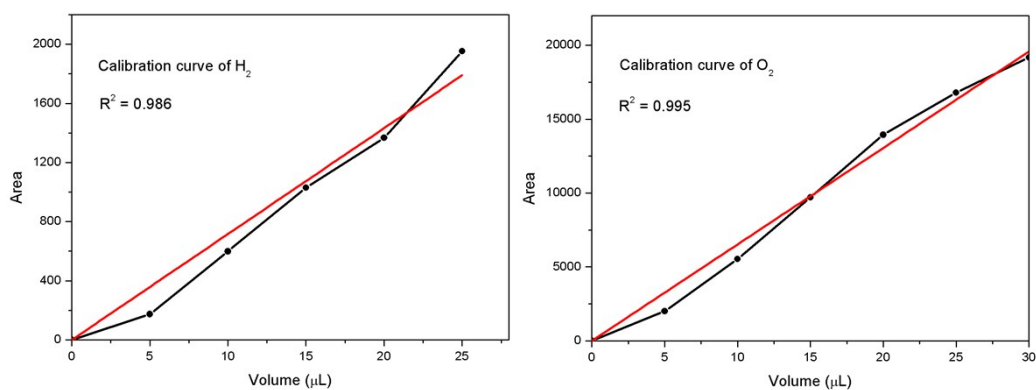
Inductively Coupled Plasma-Mass Spectrometer (ICP-MS). ICP-MS was performed on a Agilent 7500ce. Samples were dissolved in concentrated HNO_3.

Powder X-ray Diffraction (pXRD). pXRD data were obtained using a Bruker D8 X-ray Powder Diffractometer with a Cu K-α radiation source in the range $2\theta = 5$-$80°$.

Scanning Electron Microscope (SEM). SEM images and EDX spectra were obtained with a JSM 7000F microscope (JEOL) equipped with an Oxford EDX system.

X-ray Photoelectron Spectroscopy (XPS). XPS spectra were collected on a ULVAC-PHI XPS spectrometer equipped with a monochromatized 1486.6 eV Al Kα X-ray line source directed 45° with respect to the sample surface. The spectra were registered at a base pressure of $<5\times10^{-10}$ torr. Low-resolution survey scans were acquired with a 100 μm spot size between the binding energies of 1-1100 eV. Higher-resolution scans with a resolution of 0.1 eV were collected between 392-412 (for N), 525-541 (for O) and 700-740 (for Fe) eV.

Reference

(1) Hung, M.-C.; Tsai, M.-C.; Lee, G.-H.; Liaw, W.-F. *Inorg. Chem.* **2006**, *45*, 6041-6047.

(2) Chiou, T.-W. *et al. Angew Chem Int. Ed.* **2015**, *54*, 14824-14829.

(3) Jiang, N.; You, B.; Sheng, M.; Sun, Y. *Angew Chem Int. Ed.* **2015**, *54*, 6251-6254.

(4) McCrory, C. C. L.; Jung, S.; Peters, J. C.; Jaramillo, T. F. *J. Am. Chem. Soc.* **2013**, *135*, 16977-16987.
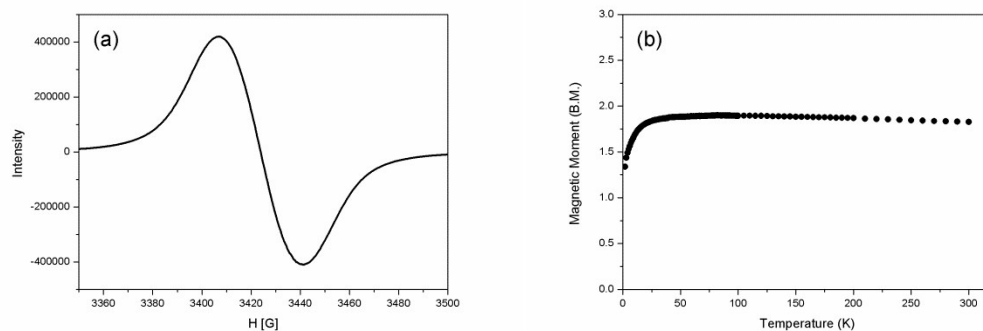
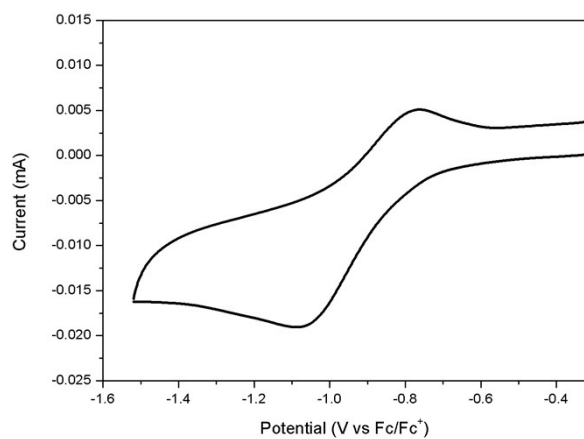**Figure S1**. (a) EPR spectrum of **2** in MeCN at 77 K. (b) Plot of magnetic moment vs temperature for **2**.

Figure S2. Cathodic cyclic voltammogram of 3-mM CH_3OH solution of **2** with 0.1 M [n-Bu$_4$N][PF$_6$] as electrolyte (E_{pc} = -1.035 V and E_{pa} = -0.766 V (vs Fc/Fc$^+$), scan rate 50 mV/s).
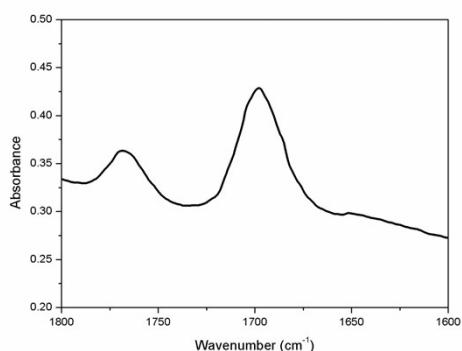
Figure S3. IR spectrum of **2** in D$_2$O solution of 1.0 M NaOH.
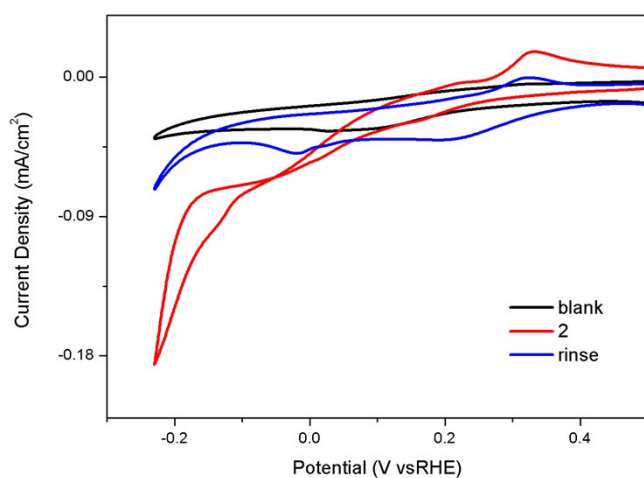
Figure S4. CV curves of blank (black), 3-mM aqueous solution of **2** (red) in 1.0 M NaOH$_{(aq)}$, and the CV (blue) obtained after CV scanning followed by rinse and subsequently transferred to fresh DNIC **2**-free aqueous solution with 1.0 M NaOH$_{(aq)}$ electrolyte for HER (scan rate 2 mV/s). (Current densities mean geometrical current densities).
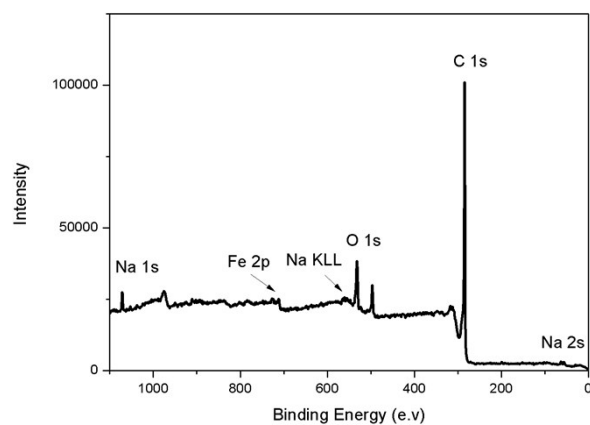
Figure S5. XPS spectrum of the graphite electrode after CV scanning for HER catalytic test in the presence of **2** (3 mM) and 1.0 M NaOH$_{(aq)}$.
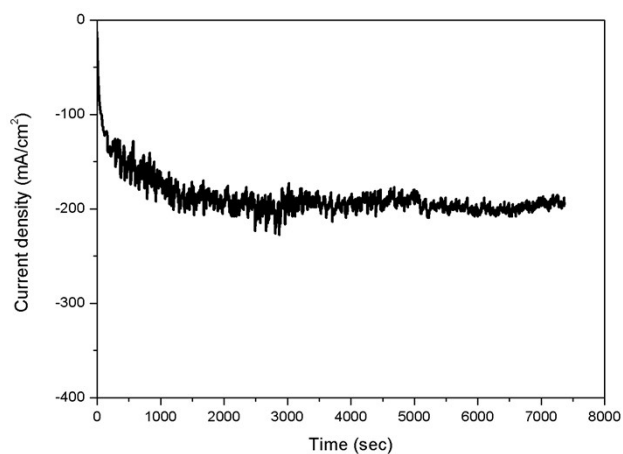
Figure S6. Increase of current density with time for the electrolysis of 3 mM **2** in 1.0 M NaOH$_{(aq)}$ at applied potential -0.48 V (vs RHE). (Current densities mean geometrical current densities).
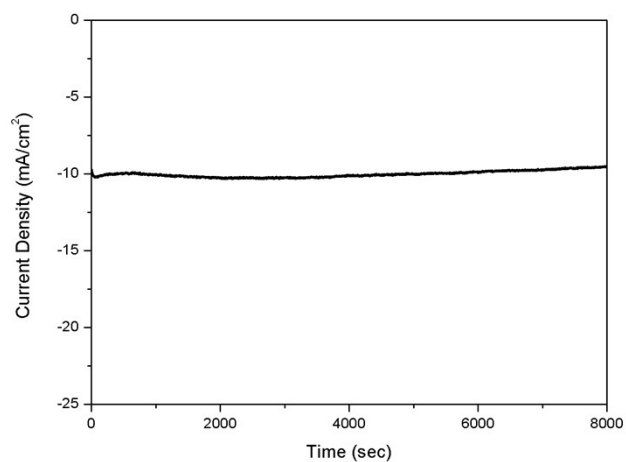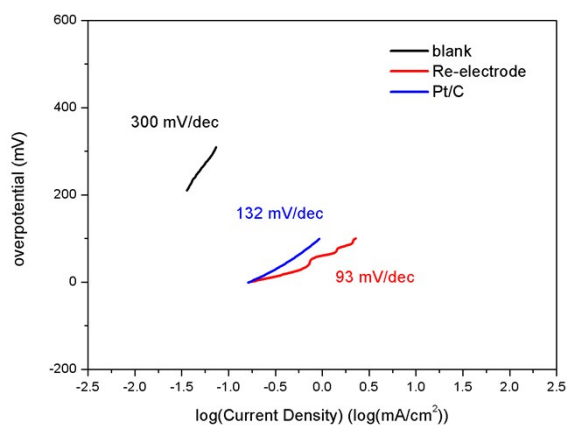
Figure S7. Current density of -10 mA/cm^2 for HER using **Re-electrode** in 1.0 M NaOH$_{(aq)}$ at applied potential -0.16 V (vs. RHE). (Current densities mean geometrical current densities).

Figure S8. The corresponding Tafel plots of blank (black), **Re-electrode** (red), Pt electrode (blue) in 1.0 M NaOH$_{(aq)}$ (scan rate 2 mV/s).
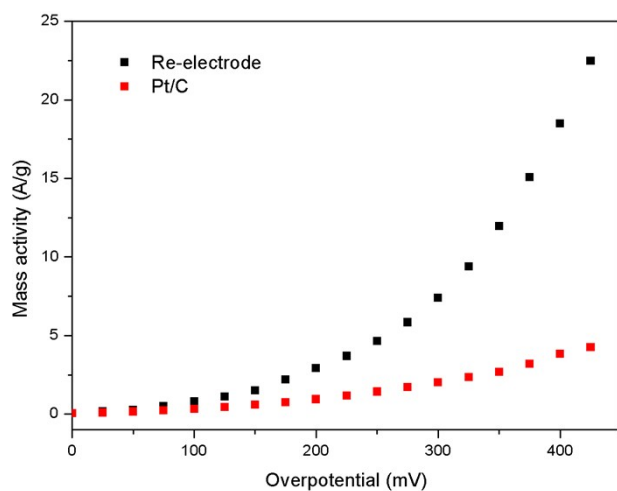
Figure S9. Mass activity as a function of the overpotential for **Re-electrode** and Pt/C.
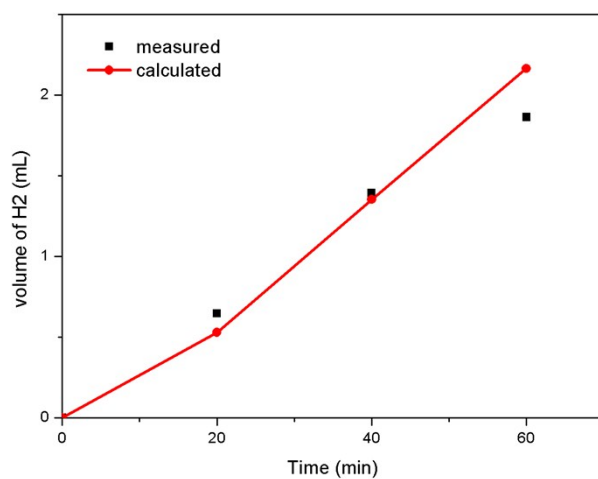

Figure S10. The amount of H_2 gas obtained by theoretical calculation (red) and experimental measurements (black) versus time for the electrolysis of 1.0 M $NaOH_{(aq)}$ using **Re-electrode** at applied potential -0.48 V (vs. RHE).
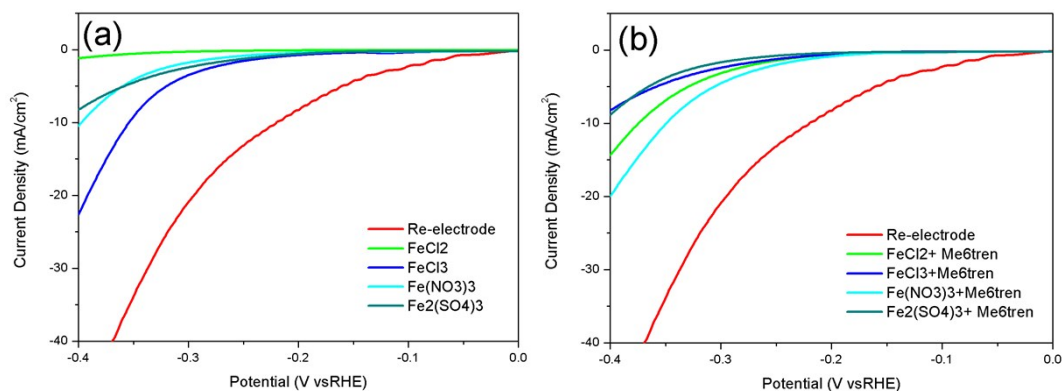
Figure S11. LSV curves of **Re-electrode** and electrodeposited electrodes of (a) Fe salts, and (b) Fe salts + Me$_6$tren ligand in 1.0 M NaOH$_{(aq)}$. The electrodeposited electrodes prepared by CPE of 1.0 M NaOH$_{(aq)}$ with Fe(NO)$_3$, Fe$_2$(SO$_4$)$_3$, FeCl$_2$, FeCl$_3$, [Fe(NO)$_3$ +Me$_6$tren], [Fe$_2$(SO$_4$)$_3$+Me$_6$tren], [FeCl$_2$ + Me$_6$tren] and [FeCl$_3$ + Me$_6$tren] (3 mM), respectively, at an applied potential -0.48 V (vs RHE) for 2 h. (Current densities mean geometrical current densities).
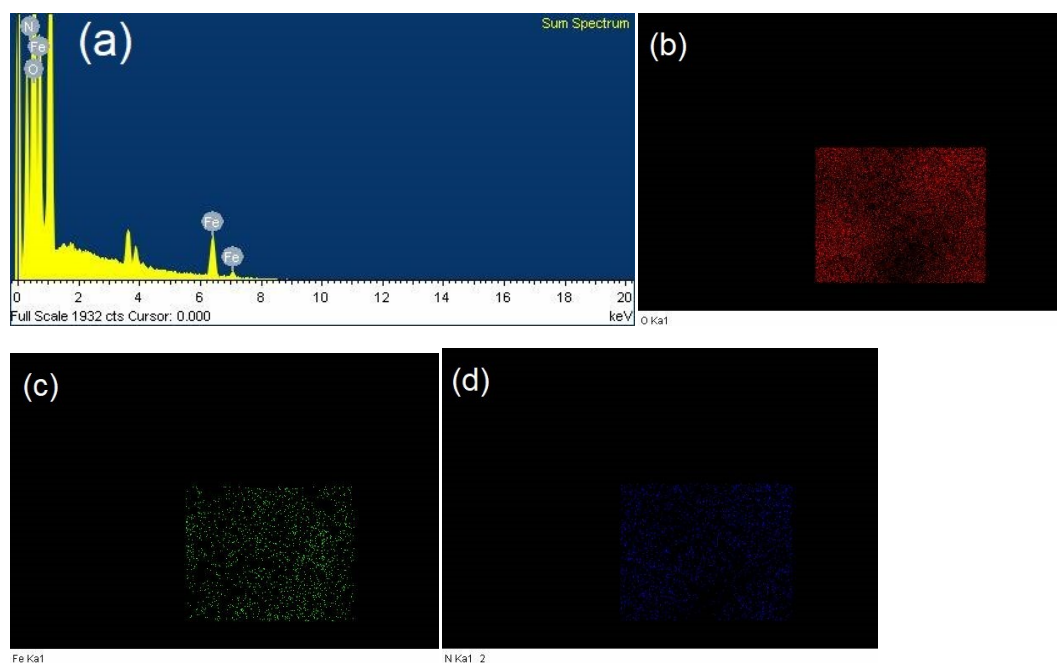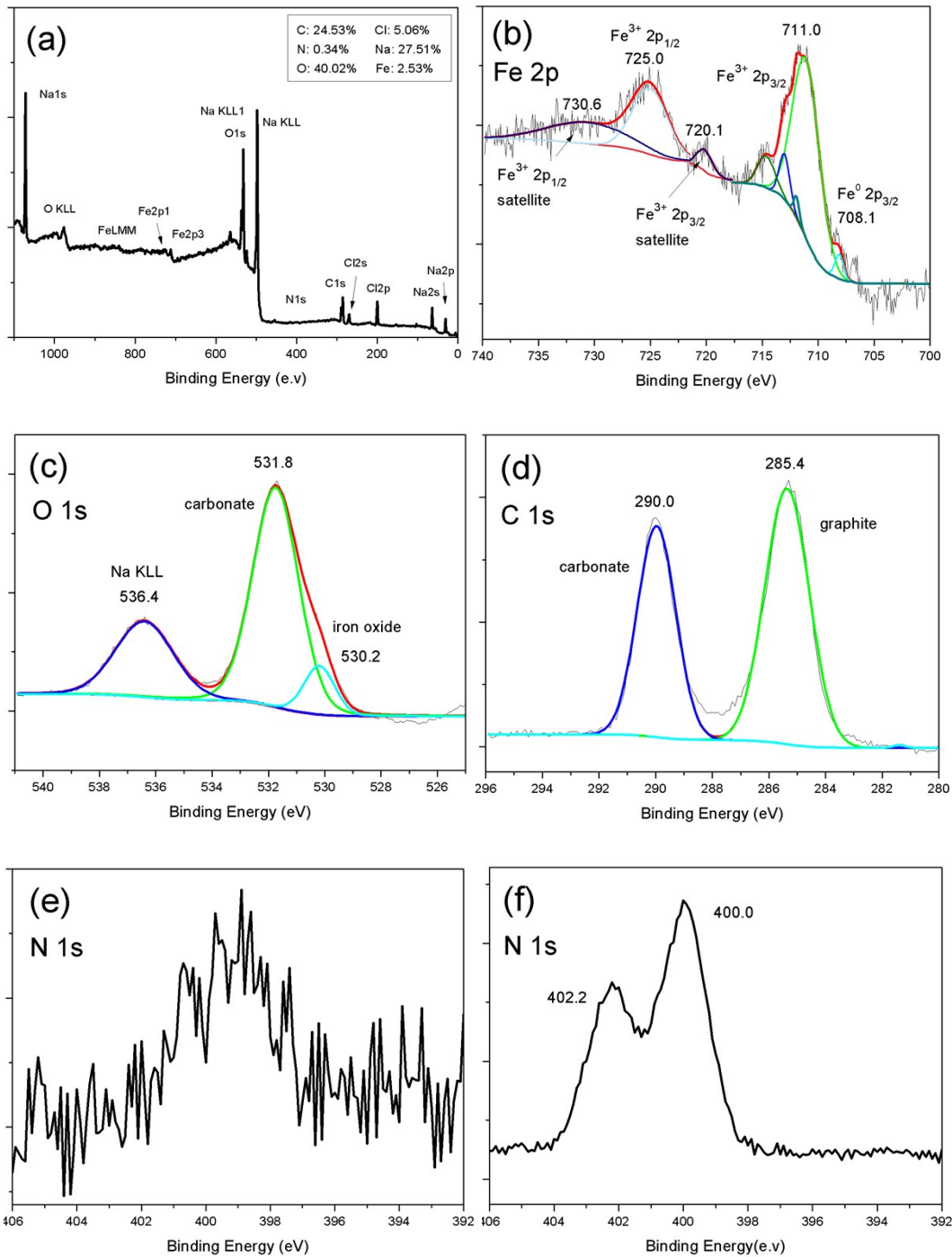

Figure S12. (a) EDX spectrum, and (b-d) SEM-EDX elemental maps (N, O, and Fe elements are shown as blue, red, and green, respectively) of **Re-electrode**.

(a)

C: 24.53%   Cl: 5.06%
N: 0.34%   Na: 27.51%
O: 40.02%   Fe: 2.53%

Na1s

O KLL
FeLMM   Fe2p1   Fe2p3

Na KLL1
O1s   Na KLL

N1s   C1s   Cl2s
Cl2p   Na2s   Na2p

Binding Energy (e.v)

(b) Fe 2p

730.6

Fe^{3+} 2p$_{1/2}$
725.0

711.0

Fe^{3+} 2p$_{3/2}$

720.1

Fe^{3+} 2p$_{1/2}$
satellite

Fe^{3+} 2p$_{3/2}$
satellite

Fe^0 2p$_{3/2}$
708.1

Binding Energy (eV)

(c) O 1s

531.8
carbonate

Na KLL
536.4

iron oxide
530.2

Binding Energy (eV)

(d) C 1s

290.0
carbonate

285.4
graphite

Binding Energy (eV)

(e) N 1s

Binding Energy (eV)

(f) N 1s
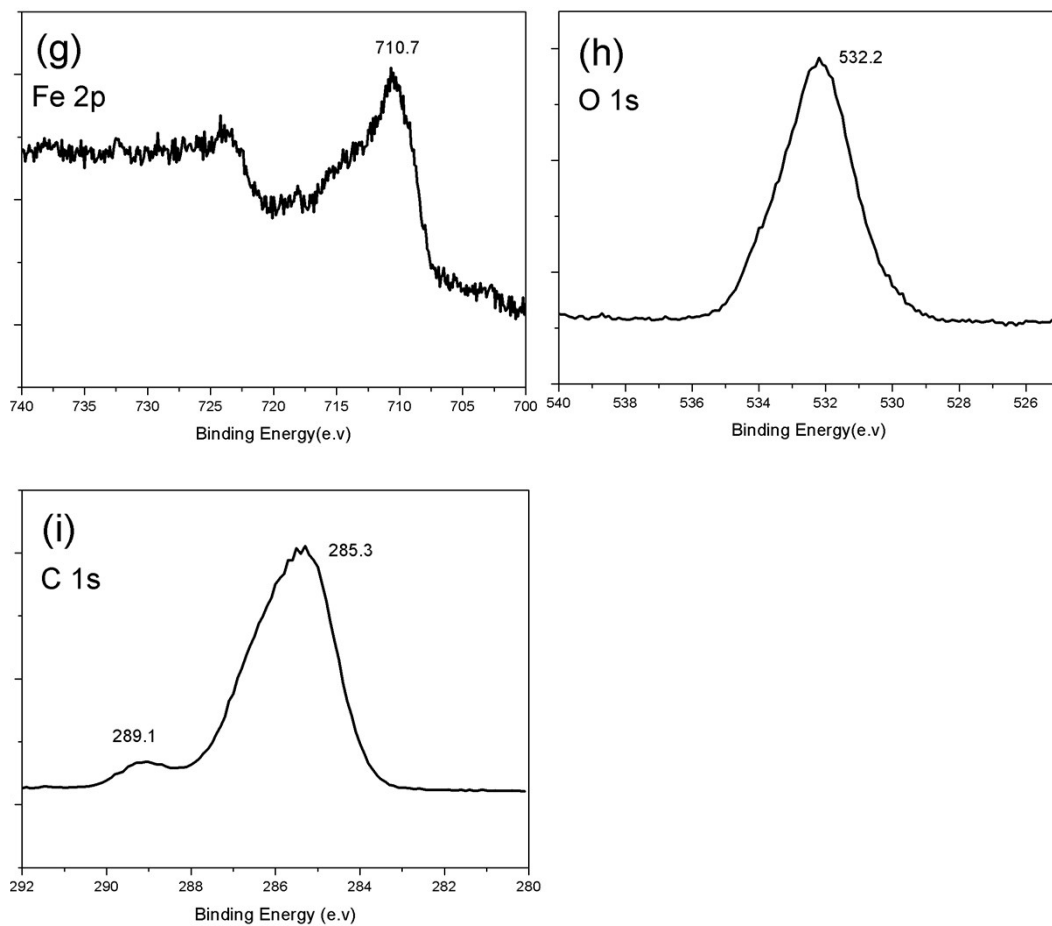
400.0

402.2

Binding Energy(e.v)

15

Figure S13. (a) Survey, (b) Fe 2p, (c) O 1s, (d) C 1s, and (e) N 1s XPS spectra of **Re-electrode** (Cl element of survey spectrum may be from SCE reference electrode). (f) N 1s, (g) Fe 2p, (h) O 1s, and (i) C 1s XPS spectra of **2**.
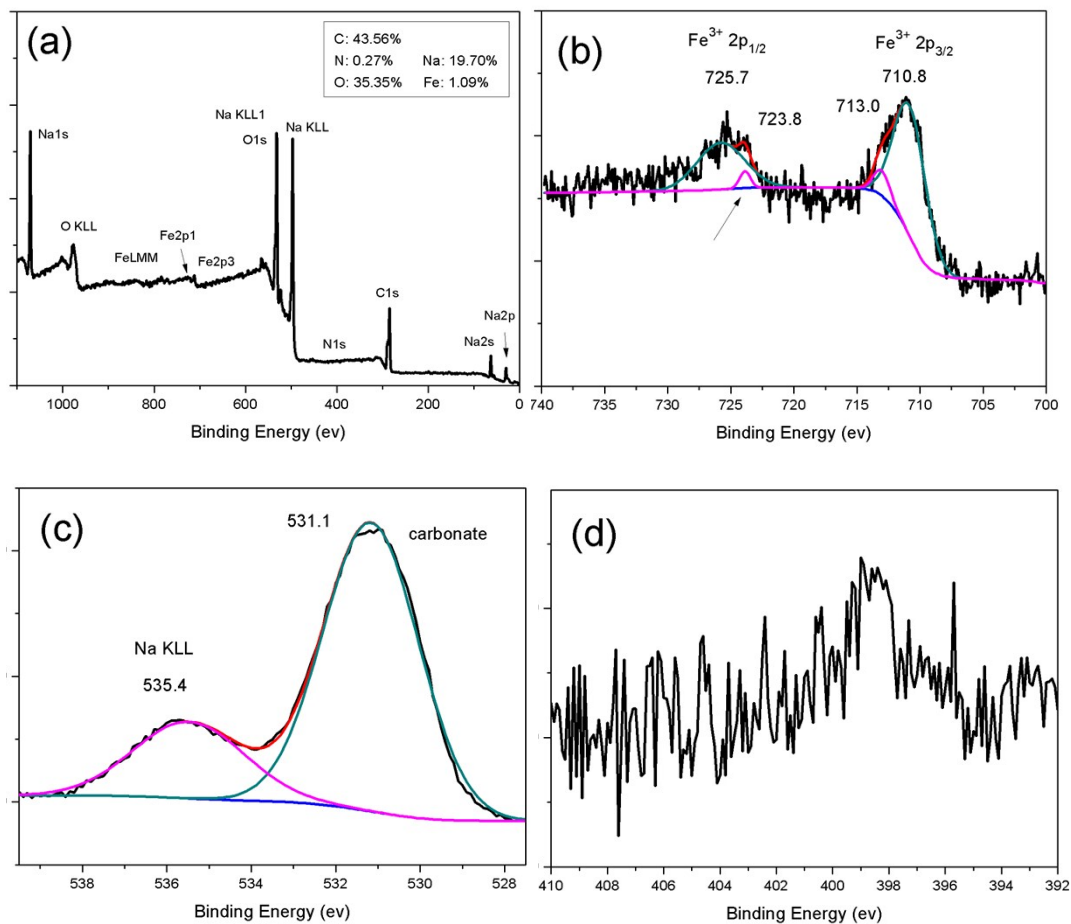
Figure S14. (a) Survey, (b) Fe 2p, (c) O 1s and (d) N 1s XPS spectra of **Re-electrode** after the CPE for 60h.
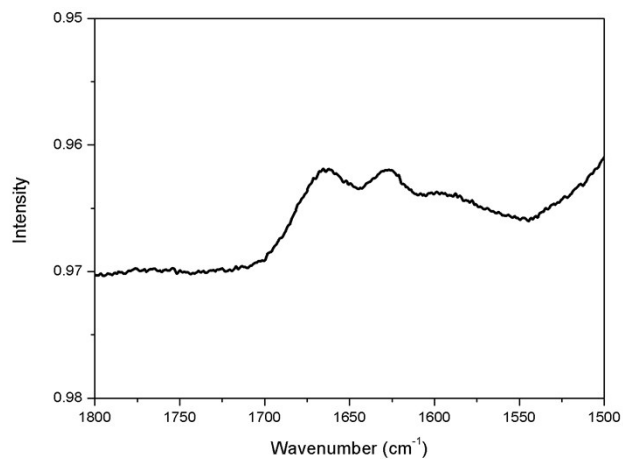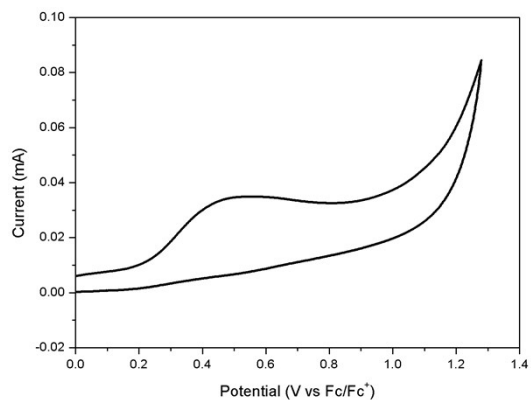
Figure S15. ATR-IR spectrum of **Re-electrode**.

Figure S16. Anodic cyclic voltammogram of CH_3OH solution of **2** (3 mM) with 0.1

M [n-Bu$_4$N][PF$_6$] electrolyte (E$_{pa}$ = 0.51 V (vs Fc/Fc$^+$), scan rate 50 mV/s).
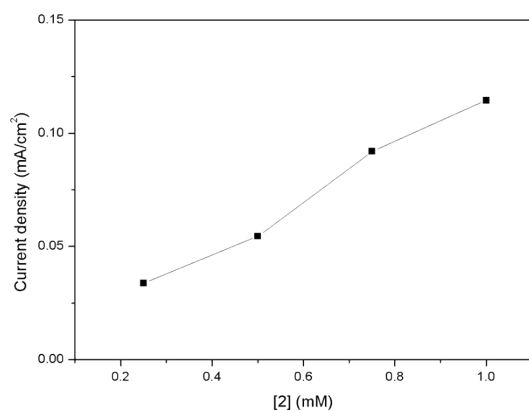
Figure S17. Dependence of the catalytic current density on the concentration of **2** in 1.0 M NaOH$_{(aq)}$ at applied potential 1.77 V (vs. RHE) for OER (scan rate 2 mV/s). (Current densities mean geometrical current densities).
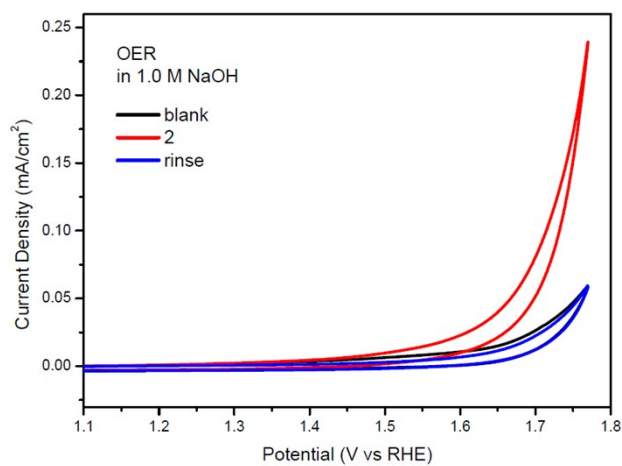

Figure S18. CVs of blank (black), 3-mM solution of **2** (red) in 1.0 M NaOH$_{(aq)}$, and the CV (blue) obtained after CV scanning followed by rinse and subsequently transferred to fresh **2**-free aqueous solution with 1.0 M NaOH$_{(aq)}$ electrolyte for OER (scan rate 2 mV/s). (Current densities mean geometrical current densities).
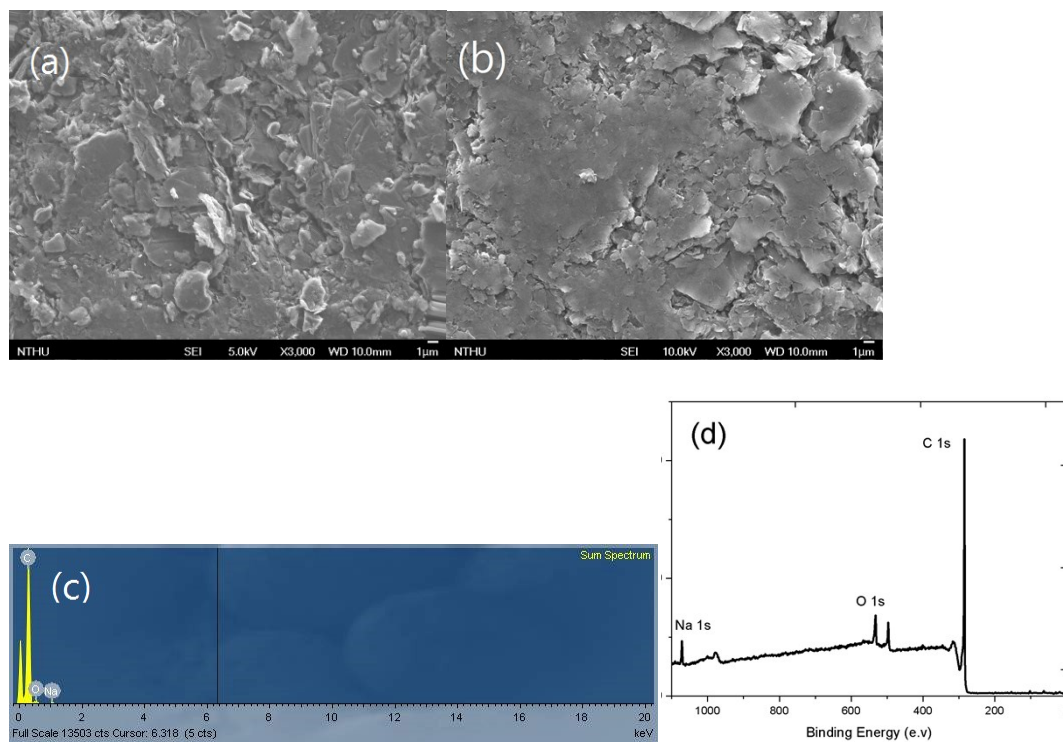
19

Figure S19. SEM, EDX and XPS spectra of the graphite electrodes (a) before and (b-d) after CV scanning OER catalytic test of **2** (3 mM) in 1.0 M NaOH$_{(aq)}$.
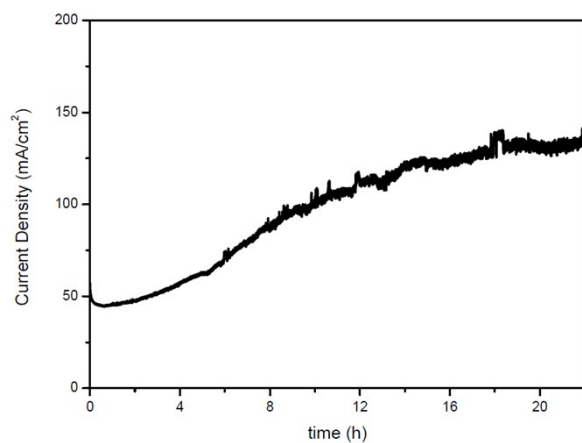

Figure S20. Changes of current density with time for the electrolysis of **2** (3 mM) in 1.0 M NaOH$_{(aq)}$ at applied potential 1.87 V (vs RHE). (Current densities mean geometrical current densities).
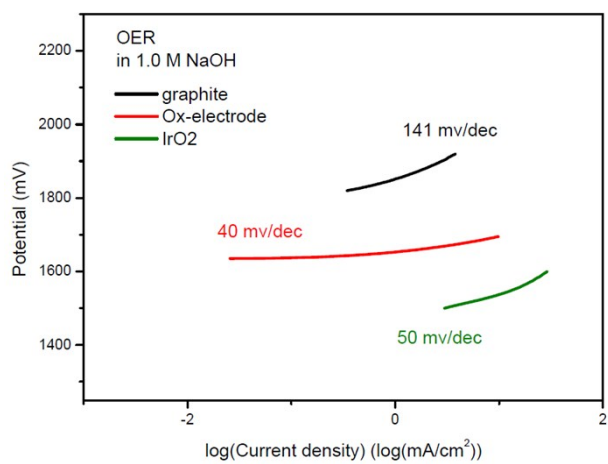
Figure S21. The corresponding Tafel plots of graphite (black), **Ox-electrode** (red) and IrO$_2$ electrode (green) in 1.0 M NaOH$_{(aq)}$ for OER (scan rate 2 mV/s).
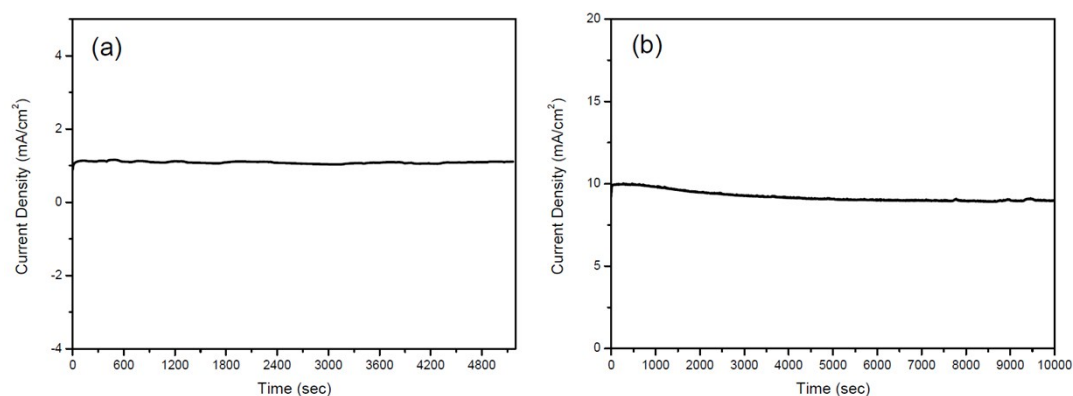
Figure S22. Current densities of 1 and 9 mA/cm^2 for OER using **Ox-electrode** in 1.0 M NaOH$_{(aq)}$ at applied potential 1.61 and 1.69 V (vs RHE), respectively. (Current densities mean geometrical current densities).

Figure S23. The amount of O$_2$ gas obtained by theoretical calculation (red) and experimental measurements (black) versus time for the controlled potential electrolysis of 1.0 M NaOH$_{(aq)}$ employing **Ox-electrode** as working electrode at applied potential 1.87 V (vs. RHE).
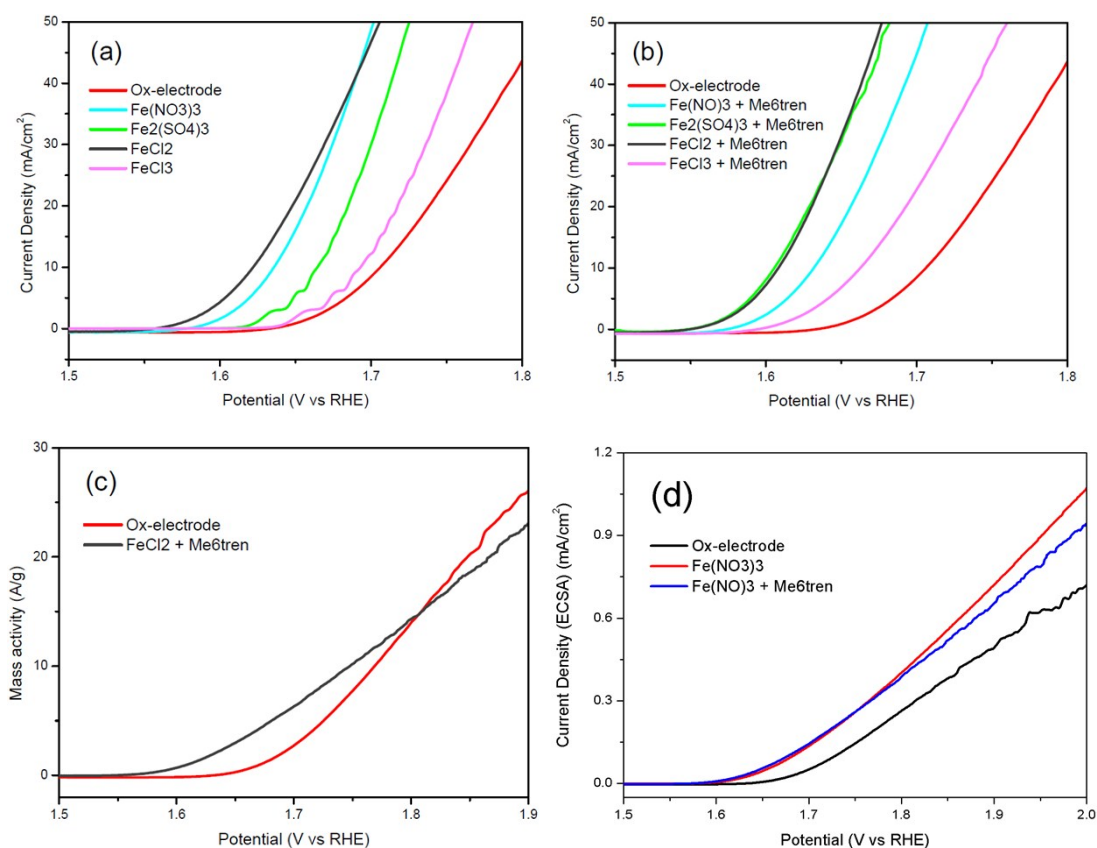
Figure S24. LSV curves of **Ox-electrode** and electrodeposited electrodes of (a) Fe salts or (b) Fe salts + Me$_6$tren ligand in 1.0 M NaOH$_{(a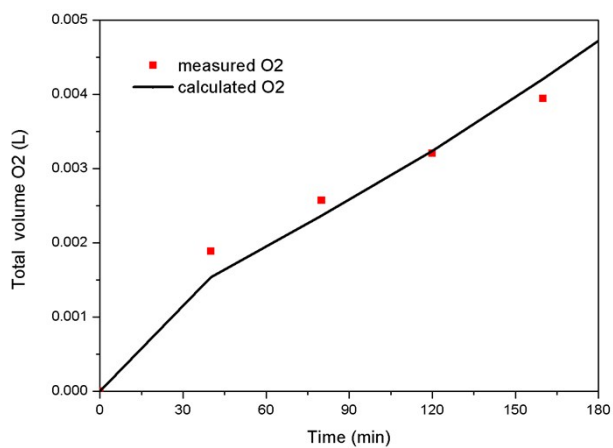q)}$. (c) LSV curves based on the active mass of **Ox-electrode** and electrodeposited electrodes of FeCl$_2$ + Me$_6$tren in 1.0 M NaOH$_{(aq)}$. The electrodeposited electrodes prepared by CPE of 1.0 M NaOH$_{(aq)}$ with Fe(NO)$_3$, Fe$_2$(SO$_4$)$_3$, FeCl$_2$, FeCl$_3$, [Fe(NO)$_3$+Me$_6$tren], [Fe$_2$(SO$_4$)$_3$+Me$_6$tren], [FeCl$_2$+Me$_6$tren], and [FeCl$_3$+Me$_6$tren] (3 mM), respectively, at applied potential 1.87 V (vs. RHE) for 22 h. (d) The LSV curves from Fig. S24a-b normalized to the electrochemical active surface area (ECSA). In Figures S24a-b, current densities mean geometrical current densities.
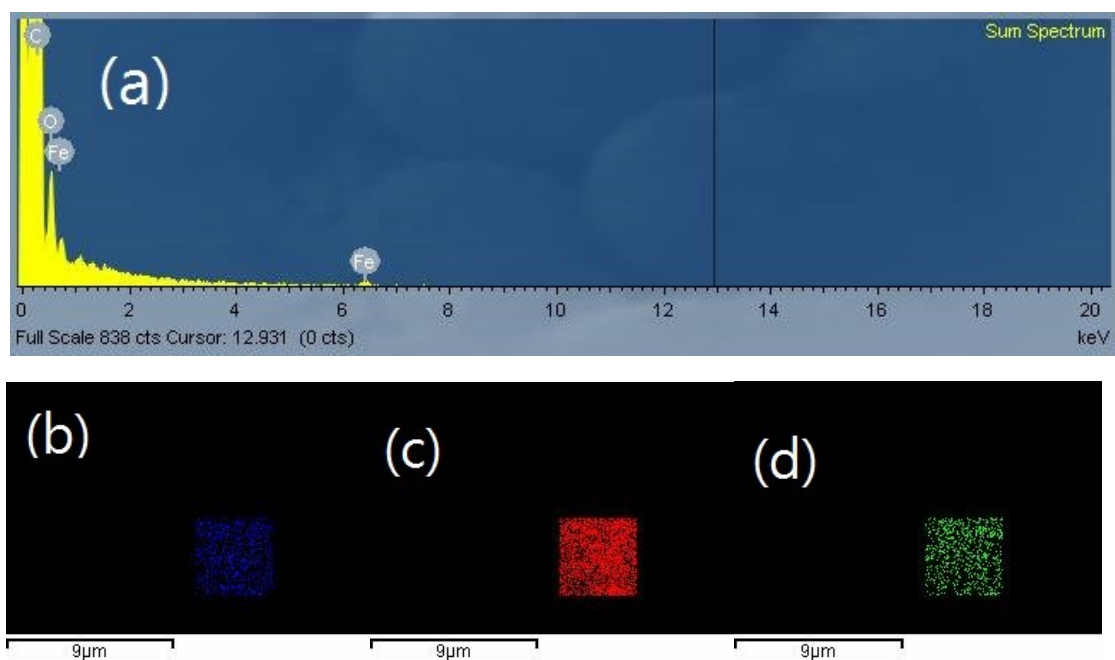
Figure S25. (a) EDX spectrum, and (b-d) SEM-EDX elemental maps (N, O, and Fe elements are shown as blue, red, and green, respectively) of **Ox-electrode**.
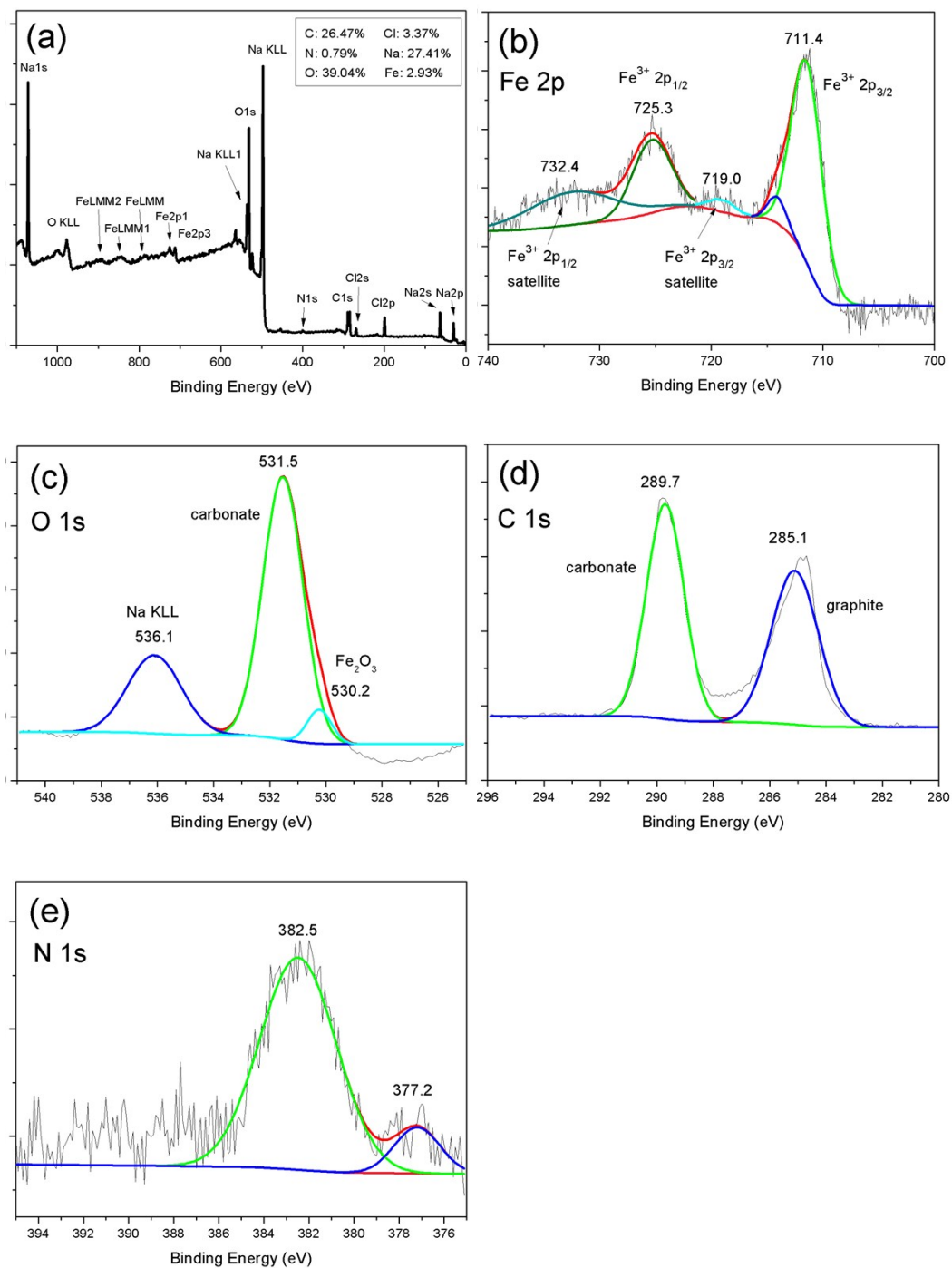
Figure S26. (a) Survey, (b) Fe 2p, (c) O 1s, (d) C 1s, and (e) N 1s XPS spectra of **Ox-electrode** (Cl element of survey spectrum may be from SCE reference electrode).
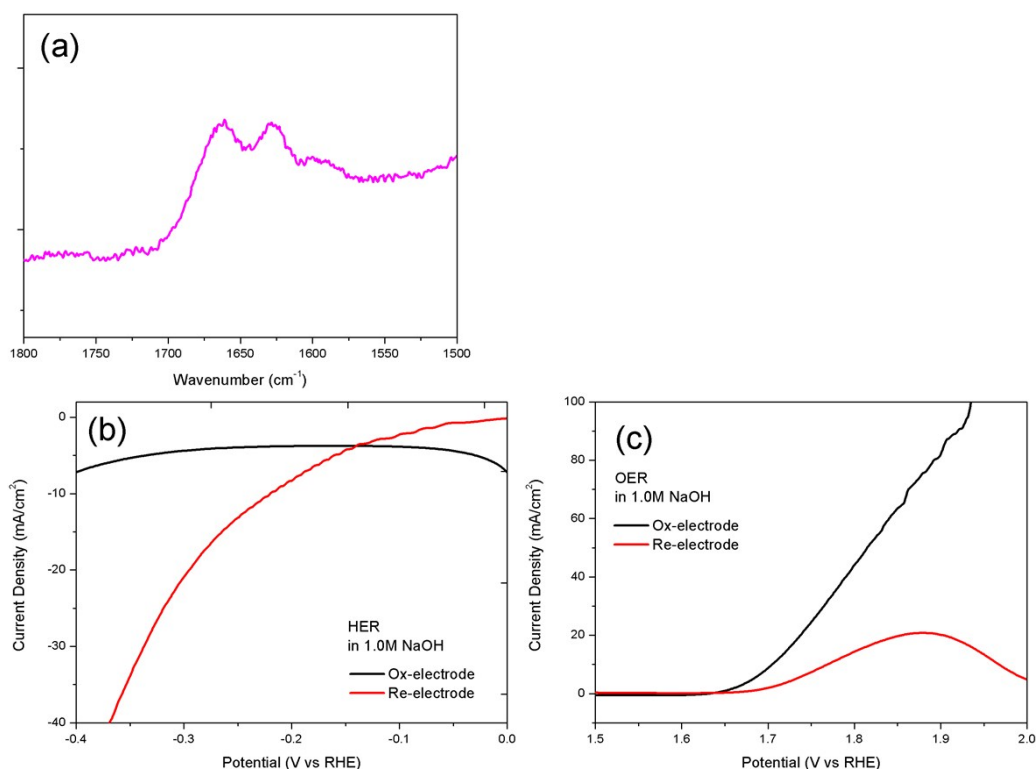
Figure S27. (a) ATR-IR spectrum of **Ox-electrode**. LSV curves of **Ox-electrode** (black) and **Re-electrode** (red) in 1.0 M NaOH$_{(aq)}$ for (b) HER and (c) OER, respectively (scan rate 2 mV/s). (Current densities mean geometrical current densities).
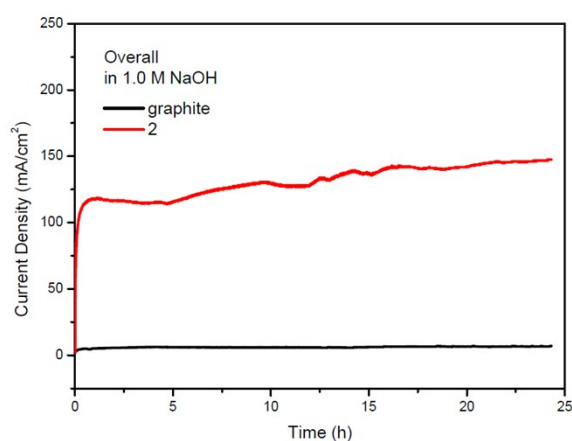
Figure S28. Changes of current density with time when graphite-electrode pair modified with CPE of blank (black) and **2** (3 mM) (red), respectively, in 1.0 M NaOH$_{(aq)}$ at applied voltage 2.20 V. (Current densities mean geometrical current densities).
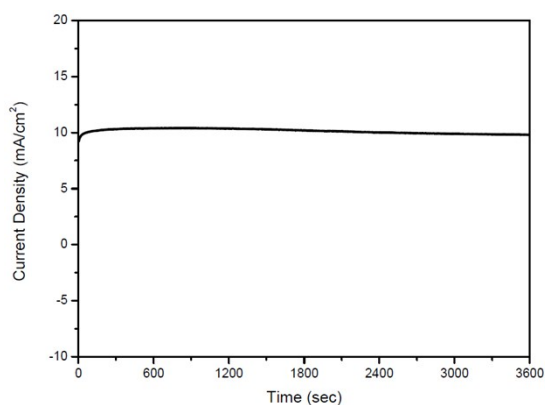
Figure S29. Current density of 10 mA/cm^2 for overall water splitting using **Redox-electrode** in 1.0 M NaOH$_{(aq)}$ at applied voltage 1.77 V. (Current densities mean geometrical current densities).
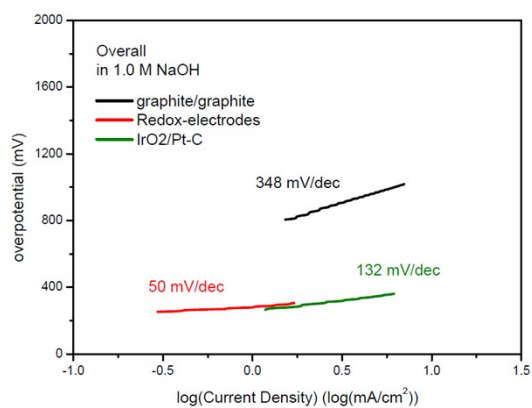
Figure S30. The corresponding Tafel plots of the fresh graphite-graphite (black), **Redox-electrodes** (red) and IrO$_2$-Pt (green) two-electrode setting in 1.0 M NaOH$_{(aq)}$ for overall water splitting (scan rate 2 mV/s).
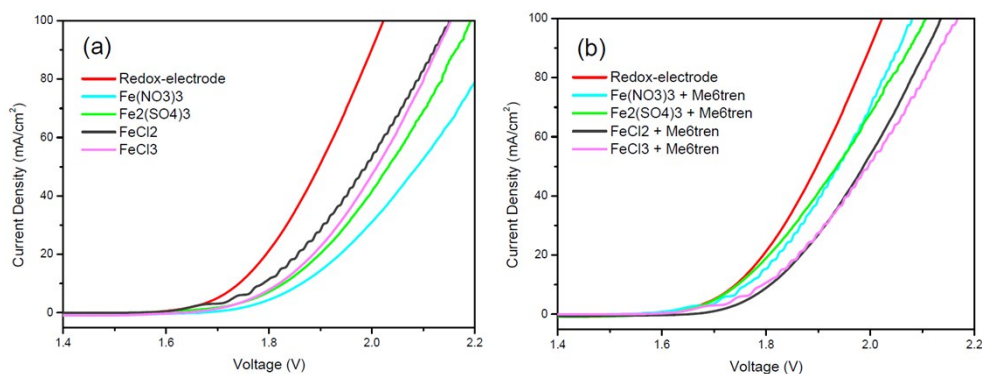
Figure S31. Polarized curves of overall water splitting for **Redox-electrode** and electrodeposited electrode-pair settings derived from (a) Fe salts and (b) Fe [salts+Me$_6$tren] in 1.0 M NaOH$_{(aq)}$ (scan rate 2 mV/s). The electrodeposited two-electrode settings prepared by CPE of 1.0 M NaOH$_{(aq)}$ with 3 mM (a) Fe(NO)$_3$, Fe$_2$(SO$_4$)$_3$, FeCl$_2$, FeCl$_3$, and 3 mM (b) [Fe(NO)$_3$+Me$_6$tren], [Fe$_2$(SO$_4$)$_3$+Me$_6$tren], [FeCl$_2$+Me$_6$tren], [FeCl$_3$+Me$_6$tren], respectively, at applied voltage 2.20 V for 22 h using graphite as both anode and cathode. (Current densities mean geometrical current densities).

Table S1. Selected Janus catalysts.

Catalysts	Voltage (V)	Current Density (mA/cm^2)	pH	Reference
Redox-electrode	1.77	10	14	This work
MoOx/Ni$_3$S$_2$/NF	1.45	10	14	Adv. Funct. Mater., 2016, 4839
N−Ni$_3$S$_2$/NF	1.48	10	14	Adv. Mater., 2017, 1701584
Ni$_2$P/NF	1.49	10	14	ACS Catal., 2016, 714
Cu@CoSx/CF	1.50	11	14	Adv. Mater., 2016, 1606200
NiFeOx	1.51	10	14	Electrochim. Acta, 2015, 297
Ni−Fe−P	1.52	10	14	J. Mater. Chem. A, 2017, 2496
CP@Ni−P	1.53	50.4	14	Adv. Funct. Mater. 2016, 4067
Ni$_x$Co$_{3-x}$S$_4$/Ni$_3$S$_2$/NF	1.53	10	14	Nano Energy, 2017, 161
Co$_2$P/CNT	1.53	10	14	Nano Energy, 2016, 303
NiFe−P	1.556	10	14	J. Mater. Chem. A, 2016, 13866
FeB$_2$	1.57	10	14	Adv. Energy Mater. 2017, 1700513
Ni(OH)$_2$@Ni/CC	1.58	10	14	J. Mater. Chem. A, 2017, 7744
NiCoP	1.58	10	14	Nano Lett. 2016, 7718
Co$_9$S$_8$@NOSC	1.60	10	14	Adv. Funct. Mater. 2017, 1606585
d-NiCo$_{0.2}$NS/Ni/CF	1.61	15	14	J. Mater. Chem. A 2016, 18499
FeNi$_3$N/NF	1.62	10	14	Chem. Mater. 2016, 6934
Ni$_{0.7}$Fe$_{0.3}$S$_2$	1.625	10	14	J. Mater. Chem. A 2017, 15838
Ni$_2$P	1.63	10	14	EES, 2015, 2347
NiCo$_2$S$_4$ NW/NF	1.63	10	14	Adv. Funct. Mater. 2016, 4661
NiCo$_2$O$_4$	1.65	10	14	ACIE, 2016, 6290
Ni$_3$N/CMFs/Ni$_3$N	1.652	20	14	Mater. Chem. Front. 2017, 2155
NiFe/NiCo$_2$O$_4$/NF	1.67	10	14	Adv. Funct. Mater. 2016, 3515
SNCF-NRs	1.68	10	14	ChemCatChem 2017, 1721
NiFe LDH/NF	1.70	10	14	Science, 2014, 1593
FeSe$_2$	1.73	10	14	ACIE, 2017, 10506
CoSe	1.75	10	14	J. Mater. Chem. A 2016, 14789
Ni$_3$S$_2$/NF	1.76	13	14	JACS, 2015, 14023
Co$_2$B-500	1.81	10	14	Adv. Energy Mater. 2016, 1502313
NFPGN	1.90	10	14	J. Mater. Chem. A 2017, 7784

N,S-CNT	2.03	10	14	Adv. Energy Mater. 2017, 1602068

Table S2. Selected HER catalysts.

Catalysts	η (10 mA/cm^2)	Tafel Slope	pH	Reference
Fe HER catalysts				
Re-electrode	160	93	14	This work
FeS$_2$	96	78	13	JACS, 2017, 13604
Vc-FeP	108	62	14	CSSC, 2017, 1509
FeP NAs/CC	218	146	14	ACScatal, 2014, 4065
Metal doping Fe HER catalysts				
FeNi3N	75	98	14	Chem. Mater. 2016, 6934
Non-Fe HER catalysts in alkaline condition				
MoNi$_4$	15	30	14	NatComm, 2017, 15437
Porous-MoO$_2$	27	41	14	Adv. Mater., 2016, 3785
NiCoP	32	37	14	Nano Lett. 2016, 7718
NiMo	34 (20)		14	ChemElectroChem, 2014, 1138
WO$_2$ HN	48	43	14	J. Mater. Chem. A, 2017, 9655
Ni$_5$P$_4$	49	98	14	EES, 2015, 1027
Cu$_{95}$Ti$_5$	60	110	13	NatComm, 2015, 6567
Ni(OH)$_2$@Ni	68	97	14	J. Mater. Chem. A, 2017, 7744
NiMo	70 (20)		14.3	ACScatal, 2013, 166
CoO	73	82	14	NatComm, 2017, 1509
MoC	77	50	14	J. Mater. Chem. A, 2016, 6006
WC-CNT	137	106	13	ACS.Nano, 2015, 5125
NiO/Ni-CNT	<100	82	14	NatComm, 2014, 4695
N-NiO	100	112.58	14	ChemSusChem, 2018, 1020
MoCx	151	59	14	NatComm, 2015, 7512
Co-NRCNT	160 (1)		14	ACIE, 2014, 4372
CoMo	170 (100)	92	14.8	J. Electrochem. Soc., 1994, 382
CoNx	170	75	14	NatComm, 2015, 7992
c-CoSe$_2$/CC	190	85	14	Adv. Mater., 2016, 7527
Ni$_2$P	205		14	JACS, 2013, 9267
NiCo$_2$S$_4$/NF	210	58.9	14	Adv. Funct. Mater., 2016, 4661

CoS_2	244	133	14	Electrochimica Acta, 2014, 170

Table S3. Selected OER catalysts.

Catalysts	η (1 mA/cm^2)	Tafel Slope	pH	Reference
Fe OER catalysts				
Ox-electrode	380	40	14	This work
FeOx	445	40	14	J. Electrochem. Soc., 2013, H142
FeOx	405	51	14	JACS, 2012, 17253
Fe$_2$O$_3$	430	64	14	NanoLett, 2014, 2123
FeOx	410	40	13	Science, 2013, 60
FeOOH	420		11	JACS, 2014, 2843
Metal doping Fe OER catalysts				
NiFeOx	297	30	14	JACS, 2012, 17253
NiFeOx	120	32	15	NatComm, 2015, 6616
NiFeOx	210	31	14	JACS, 2013, 8452
Fe$_2$Ni$_3$Ox	250	34	13	JACS, 2013, 11580
FeCoW oxyhydroxides	191 (10)		14	Science, 2016, 333
Ba$_{0.5}$Sr$_{0.5}$Co$_{0.8}$-Fe$_{0.2}$O$_{3-\delta}$	320	60	13	Science, 2011, 1383
α-Fe$_{33}$Co$_{33}$Ni$_{33}$Ox	230	30	13	Science, 2013, 60
Non-Fe OER catalysts				
NiCoOx	312	33	14	JACS, 2012, 17253
NiCoOx	370		13	ChemComm, 2015, 9511
NiMnOx	300	47	14	J. Mater. Chem. A, 2015, 20056
NiCoCeOx	250	60	14	EES, 2014, 682
Co$_3$O$_4$	300	49	14	Chem. Mater., 2012, 3567
CoP	345 (10)	47	14	ACIE, 2015, 6251
CoMnP	330 (10)	61	14	JACS, 2016, 4006
NiOx	320 (10)	52	14	JACS, 2016, 6517
MnOx	<300		13	JACS, 2010, 13612
NiOx	380	30	9.2	JACS, 2013, 3662
CoOx	410	60	7	Science, 2008, 1072